Rev. Adv. Mater. Sci. 29 (2011) 54-67

BEHAVIOR OF RADIATION DEFECTS IN NANOMATERIALS

R.A. Andrievski

Institute of Problems of Chemical Physics, Russian Academy of Sciences, Semenov prospect, 1, Chernogolovka, Moscow Region 142432, Russia

Received: March 23, 2011

Abstract. The much attention is given to some possible results of the nanomaterials irradiation such as the interphase role as the radiation defect sinks, the nanostructure amorphization, the nanocrystallization of amorphous state, the alloying component segregation, and the enhancement of recrystallization. The radiation effects are analyzed in connection with the structure and physical/mechanical properties of nanomaterials-based metals, alloys and compounds (intermetallics, nitrides, oxides, carbides). The results of microscopic approaches and the molecular dynamics modeling are also described. Some low investigated questions are pointed and discussed.

1. INTRODUCTION

The nanomaterials are the non-equilibrium objects in general due to the great interface presence (including concentration segregations, residual stresses, etc.) and it causes to relate with a special attention to the real exploitation conditions influence on these materials structure and properties. It is obvious that such objects under the thermal action or the stress, corrosion and radiation fields will suffer some processes connected with recrystallization, segregation, homogenization and relaxation, phase transitions, phase decay and arising, amorphization, sintering and filling of micro- and nanopores (nanocapillars). All these processes lead to a nanostructure evolution or even to its annihilation that is accompanied with the changes of its physical, chemical, mechanical and other properties. The questions of the nanostructures stability are of special interest because this problem has not only a theoretical value but have the big applied importance too, for both the nanomaterial stability and their economic effectiveness predictions [1-4].

The information about the nanomaterials behavior under an irradiation is very important especially for the design and creation the perspective materials for the nuclear units new generation (fast-neutron reactors, high-temperature gaseous reactors, thermonuclear reactors, etc), because their operational conditions presuppose a long-term exploitation in the strong radiation fields under the high temperatures, severe stresses and corrosive surrounds. The new materials for the nuclear and thermonuclear power engineering must be very stable ones.

The simplest picture of the radiation defects arise into usual metals assumed that under the material bombardment by high energy particles or neutrons the energy is partially transmitted to the displaced atoms of the crystal lattice and the primary knock-on atoms (PKA) are arising. The so called displacement cascades involve the Frenkel pairs in a form of the interstitial atoms and vacancies (IAV), their complexes (clusters) in a form of loops and the vacancies nanopores. The point radiation defects can mutually recombinate (annihilate), are absorbed by pores and dislocations or remove along the interfaces acting in this instance as the sinks. The irradiation leads to the next main changes in the material structure: an amorphization, a ductility decrease

Corresponding author: R.A. Andrievski, e-mail: ara@icp.ac.ru

© 2011 Advanced Study Center Co. Ltd.

(the radiation hardening) and an embrittlement (with a possible rise of the creep rate at high temperatures) due to the defect content increase. In addition, there can be observed a swelling (the volume increase due to the non-compensated vacancy sinks) and a transmutation due to the nuclear reactions or radioactive decay. The radiation processes in the nanoobjects under study until now had not been adequately investigated (as compared with the usual coarse crystallized materials, see for example [5,6]), and the study of the radiation defects in nanomaterials is still in its infancy [4,7].

From the general considerations and existing experimental data the following next scenario can be proposed for the nanomaterials behavior under an irradiation:

- the great quantity of the interfaces (in the forms of the grains and triple joints boundary) can function as the sinks for the radiation defects removal and it leads to the nanomaterial stability increase as compared with the usual coarse-grained materials;
- the radiation defects will assist the nanostructure annihilation and its transformation to an amorphous state;
- the irradiation will give rise of the recrystallization processes;
- the alloying component segregation can be significant in irradiated nanomaterials;
- the nanocrystallization induced by irradiation can be observed in metallic glasses.

As it will shown below all these scripts (some of them is contradictory one to another) take places and must be considered by different approaches.

2. EXPERIMENTAL RESULTS

As far as is known the higher radiation stability (as compared with the coarse-grained materials) was firstly marked for the nanocrystalline samples of ZrO_2 and Pd at irradiation by Kr ions [8,9], when the interface role (as the sinks for the radiation defects) manifests itself clearly. In Fig.1 the radiation defect density into the irradiated samples of ZrO_2 and Pd is shown depending on the grain size *L*. The defects were indicated by a deformation contrast in transmission electron microscope (TEM). The results show that the defects are not present for the grain sizes below 15 nm (ZrO_2) and 30 nì (Pd), i.e. they either are passing out the sample sizes along the interface boundaries and/or are regenerating on the grain boundaries. The difference between the defect-free grain sizes of ZrO_2 and Pd reflects the higher diffusion mobility of the point defects in palladium comparing with zirconium oxide. At present time, the methods of the irradiated materials investigation are broadened and now they include not only using the accelerators but the irradiation by neutrons in the reactor conditions. In Table 1 some results of the nanomaterials irradiation are presented. For comparison the data are given concerning the coarse-grained materials irradiation.

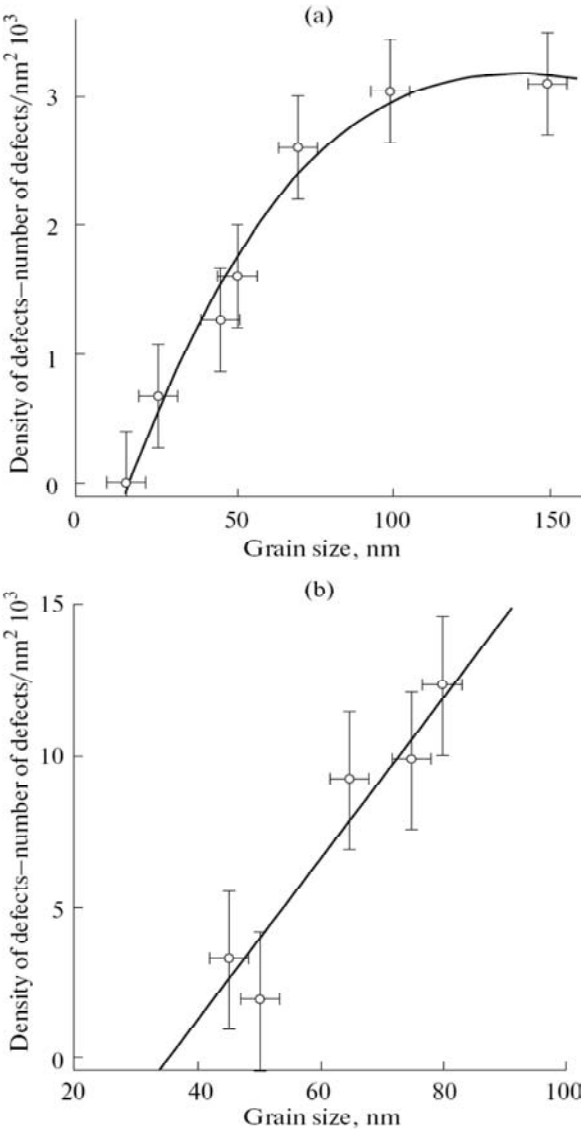

Fig. 1. The nanocrystallites size influence on the radiation defects concentration in zirconium oxide (a) and palladium (b). Irradiation by Kr ions (ZrO_2 - E = 4 MeV, dose 3-8 dpa; Pd - E = 0.24 MeV, dose 110-210 dpa), data from [9]. Reprinted with permission from M. Rose, A.G. Balogh and H. Hahn, Nuclear Instruments and Methods in Physics Research Section B 127/128 (1997) 119, © 1997 Elsevier Science.

Table 1. Effect of the irradiation by ions at accelerators and neutrons in reactor conditions on nanomaterials (dpa – displacements per atom).

Subject	Grain size, nm	Particle	Irradiation conditions Energy (MeV); Temperature (K)	Dose (dpa); fluence (ions/cm^2;n/cm^2)	Result
$MgCa_2O_4$ [10]	4-12	Kr	0.3;100	12-96 dpa	Nanocrystals are stable to amorphization
	~10^4				Amorphization starts at the dose of 12 dpa
TiNi [11]	31±6	Ar	1.5;293	0.2-5.6 dpa	Amorphization is not observed
	$8\cdot10^4$				Amorphization starts at the dose of 0.4-2.5 dpa
3C-SiC [12]	36	Au	4;293	10^{13}-10^{15} ions/cm^2	Amorphization starts at the fluence of 10^{14} ion/cm^2
	~10^3				Amorphization starts at the fluence of 10^{13} ion/cm^2
W-0.3%TiC [13]	50-200	He	3;823	Up to 2 x$\cdot10^{19}$ ions/cm^2	Blistering is observed at the fluence of 10^{19} ion/cm^2
	Conventional W				Blistering is observed at the fluence of 10^{18} ion/cm^2
W-0.5%TiC [13]	50-200	Neutrons	> 1;873	$2\cdot x10^{20}$ ions/cm^2	Radiation hardening is not observed
	Conventional W				Hardness is increased up to 20%
Nanostructured ferritic steel 14 YWT [14]	~500 (grains); 2-5 (inclusions)	Neutrons	> 0.1; 573-900	1.5 dpa	Small radiation hardening and little loss of ductility

The results show that a nanostructure positive influence at the ion and neutron irradiation is fixed for the consolidated nanoobjects with various bonding nature (complex oxide $MgCa_2O_4$, intermetallic compound TiNi, cubic modification of silicon carbide, disperse hardened tungsten, nanostructured chromium steel). In all cases the amorphization and radiation hardening are absent and the blistering (a surface spalling) manifests itself to a lesser degree. The analogous results were obtained for the nanocrystalline samples of nickel, copper and chromium-nickel stainless steel (see, for example [15,16]).

The mechanical properties change under irradiation was most extensively studied for the ODS-EUROFER and 14YWT ferritic/martensitic steels [17]. Former is an European variant of the oxide dispersion strengthened (ODS) steels that is produced by mechanical alloying small amounts (0.2-0.3 wt.%) of Y_2O_3 powder with gas atomized EUROFER 97 powder followed by consolidation using hot isostatic pressing. The 14YWT steel is a nanostructured ferritic/martensitic steel (Fe-14 wt.%Cr-3W-0.4Ti) obtained in the Oak Ridge National Laboratory. Its powder with 0.3 wt.% of Y_2O_3 nanoparticles was mechanically alloyed using high-energy attritor type ball mill and consolidated by hot extrusion at 850 °C with the following repeated hot rolling. Such consolidation regime allows to create a matrix structure with the submicron size grains that is near to nanocrystalline structure. As is shown in Fig.2, the grain sizes are between 100 – 1000 nm, the relation length to width for the grains is about 1 – 5 and the oxide inclusions size is about 2 – 5 nm.

The test results for the initial and irradiated samples are presented in Table 2, they demonstrate the mechanical characteristics advantage of the

Table 2. Yield strength (σ_Y), ultimate strength (σ_B), total elongation (δ), fracture toughness (K_{IC}) at room temperature, and temperature of ductile-brittle transition (T_{DBT}) of ODS-EUROFER and 14YWT steels in unirradiated and irradiated conditions (E > 0.1 MeV, dose 1.5 dpa, T = 573K) [17].

Steel	Condition	σ_Y (MPa)	σ_B (MPa)	δ (%)	k_{IC} (MPa·m$^{0.5}$)	T_{DBT}(° C)
ODS-EUROFER	Unirradiated	966	1085	11.7	160	–115
	Irradiated	1243	1254	7.1	180	–30
14YWT	Unirradiated	1435	1564	12.0	180	–188
	Irradiated	1560	1641	7.4	225	–175

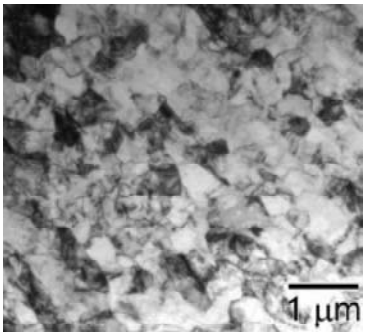

Fig. 2. Bright-field TEM-image of the 14YWT steel structure [14]. Reprinted with permission from D.A. McClintock, D.T. Hoelzer, M.A. Sokolov and R.K. Nanstad, J. Nucl. Mater. 386-388 (2009) 307, © 2009 © 2010 ELSEVIER BV.

14YWT nanostructured samples over the more coarse crystalline ODS-EUROFER objects both in the initial and irradiated states. Of particular interest is that the irradiation weakly affects on the temperature of ductile-brittle transition and a high value of fracture toughness that can be connected with the good cohesion of the oxide nanosize inclusions (of $Y_2Ti_2O_7$ and Y_2TiO_5 type) with the matrix. The volume content of such inclusions is about 1.4x 10^{-24} m^{-3} and they are characterized by a high thermal stability up to 1000 °C [18]. The irradiation of the 14YWT steel samples at temperature up to 900Ê and the characteristics study in a wide temperature range (from nitrogen ones up to 900Ê) also had demonstrated a high radiation stability of this material [17].

The detailed survey of technology and characteristic of the Japanese nanostructured ferritic steels MA957 and J12YWT was presented in [19]. Apart from the mentioned high thermal stability of the MA957 steel (Fe-14Cr-0.9Ti-0.3Mo-0.25Y_2O_3; extrusion at 1150 °C; the grain sizes from 200 to 1000 nm, the relation length to width for the grains about 1 – 5 and the mean diameter of oxide inclusions 2.1±0.4 nm) [18], the interesting results were obtained from the radiation resistance tests. The neutron irradiation at T = 370-750 °C (doses up to 40 dpa) and T = 500-750 °C (doses up to 100 dpa), as well as the irradiation by heavy ions at 670 °C (doses up to 150 dpa) have revealed the slight changes of the dislocation and grain structures for MA957 steel. The study of creep under the irradiation at T = 400-600 °C revealed its non-thermal nature. It was marked also a radiation hardening decreasing with the temperature rise. More detailed study of the helium pores had shown that in the irradiated nanostructured steels the He concentration (and their brittle decay correspondingly) can be regulated using the interface surfaces. At the same irradiation doses the He concentration in MA957 steel is less than in EUROFER97 steel by a factor of three. In general these investigations leads to the conclusion that the radiation stability of MA957 steel is sufficiently high but the irradiation is attended with some accumulation of the radiation defects [19].

The tomographic atom probe methods are used in studies of the irradiated material properties in general (and the steels especially). These methods allow trace the behavior and segregation of the doping elements under the radiation processes (e.g., see [20,21]). It was found that an irradiation by ferrous ions (E = 0.16 MeV, dose 5-10 dpa) the nanostructured 316 austenitic stainless steel leads to the grain boundary depletion by chromium and their enrichment by nickel and silicon [20]. Tomographic atom probe characterization of ODS EUROFER steel revealed that fast neutron irradiation (T = 330 °C, the dose up to 32 dpa) leads to the concentrations change of nanoclasters (with diameter 1-3 nm; their number density is 2-4 x 10^{24} m^{-3}) as compared with unirradiated state [21]. Irradiation resulted in escaping vanadium from clusters into surrounding matrix. The concentrations of yttrium and oxygen in the matrix increase after irradiation by six and three times (respectively) as a possible result of dissolution of the Y_2O_3 nanoparticles.

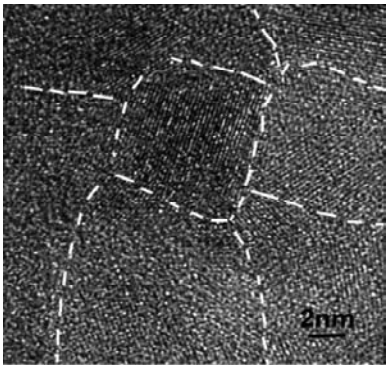

Fig. 3. High resolution TEM-image of an ion-irradiated TiN film (deposited and irradiated at room temperature by helium ions) [28]. Reprinted with permission from H. Wang, R. Araujo, J.G. Swadener, Y.Q. Wang, X. Zhang, E.G. Fu and T. Cagin, Nucl. Instr. Meth. Phys. Res. B.261 (2007) 1162, © 2007 Elsevier Science.

The radiation induced chromium and silicon segregations were discovered by the X-ray emission spectroscopy method on the surface of the ferritic/martensitic steel samples after an irradiation by Ni (E = 7 MeV) and He (E = 30-70 KeV) ions [22]. The investigations of the radiation-induced segregations in nanomaterials are only beginning and an understanding of such materials strength or their corrosion characteristics nature under irradiation will be obtained in future.

It must be noted that ODS type steels have long been developed in former USSR (Russia, Ukraine (e.g., see [23-25]). The low temperature electron (E = 5 MeV) and neutron (E > 0.1 MeV) irradiation of ODS steel K5 (13Cr1TiMo-Y_2O_3) and the model ferritic steels (Fe-2, 13, and 20 Cr) had shown that there is not any qualitative difference in the radiation defects behavior in these objects [25]. The irradiation at T = 77K leads to a sufficient radiation embrittlement and a strong decrease of the plasticity characteristics. The study of the irradiated sample electric and mechanical properties allow to register an overlapping of the displacement cascades under a neutron fluence more than 1.5×10^{14} m^{-2}. A comparison between the annealed samples being irradiated by electrons and neutrons shows an agreement of the defect behavior regularities under the cascade and cascade-less (electronic) irradiations.

In general, it can be said that the creation and studies of the matrix nanostructures had received the little researchers attention though more then 20 years ago it was shown that the radiation swelling can be limited by a non-traditional method using a batten (rod) structure with a high density of the interface boundaries in the austenitic/martensitic Cr16Ni19Mo3 and Cr13Mg7V2 steels [26,27].

The interesting results were obtained for the films being irradiated by the accelerators. In Fig. 3 the high resolution TEM-image of the nanostructured TiN film, irradiated by He ions flow (E = 12 keV, total fluence of·10^{16} ions/cm^2; T = 293K) [28] As indicated in the figure, at the boundaries of the L~8 size crystallites boundaries the amorphization signs are absent and therefore the authors [28] correctly reasoned that it is a manifestation that the grain boundaries are functioning as the sinks for radiation defects. The films electrical resistance measurements have revealed only a little rise after the irradiation and it once more attested that the radiation defects are removed in a large extent. The X-ray and electron microscopy studies (including the surface investigation by an atomic force microscopy) of the TiN films (thickness 240 nm; L = 13-16 nm; deposited on Si at T = 293K and 423K) have shown that the argon ions irradiation with energy E = 120 keV with the fluence rise from 10^{11} ions/m^2 to 10^{12} ions/m^2 is accompanied by a decrease of the lattice period, grain sizes and surface roughness as well as an increase of the microstresses and dislocations density [29]. An amorphization was not observed in the studied fluence interval but a partial disappearing of the films columnar structure was marked that can be connected with the peculiarities of the radiation defects removal.

Very interesting results were obtained in work [30], the authors of which irradiated the multiplayer Cu/V films (with different thickness of the individual layers, from 1 to 200 nm, and a total thickness 1.5-2 μm) at room temperatures by helium ions (E = 50 keV, total fluence of 6×10^{20} ions/m^2). In this system copper and vanadium are forming an immiscible system that is a very convenient object for studying the interfaces influence by changing of the layers number in the films. In Figs. 4a and 4b it is shown that the decrease of the individual Cu/V layers thickness h leads to a decrease of the helium pores content and swelling under the irradiation. An estimation of these values (from the rule-of-mixture considerations for the individual Cu and V layers) gives the far exceeding values by comparison with the experimental data for the multilayer films.

The hardness changes of the initial and irradiated multiplayer films with the thickness h decrease is shown in Figs. 4c and 4d, demonstrating that the difference of the hardness between the initial and irradiated films is lowered with the h decrease and becomes vanishing small at h = 2.5 nm, i.e. a ra-

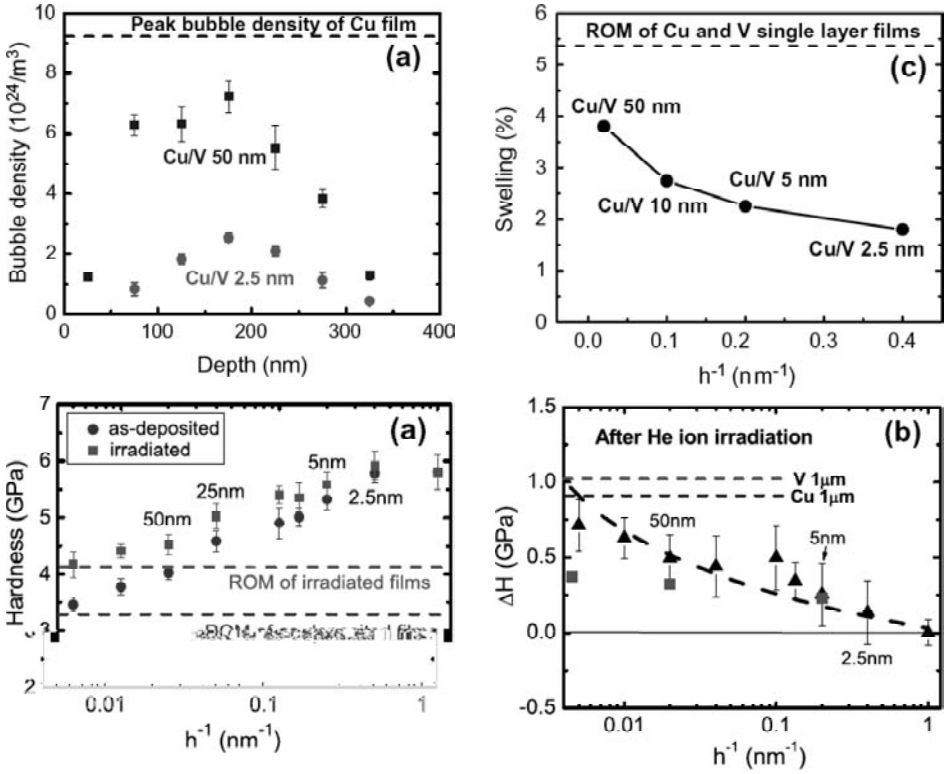

Fig. 4. The density change of the helium pores on the film depth (*a*, ■ – Cu/V *h* = 50 nm; ● – Cu/V *h* = 2.5 nm) and swelling (b), hardness (c, ■ – irradiated films; ● – as-deposited films) and the hardness change ΔH (d) under irradiation in dependence on thickness (*h*) of individual layers in the Cu/V multilayer [30]. The rule-of-mixture (ROM) swelling (Fig. 4b) and hardness (Fig. 4c) values are corresponding to single layer films. The peak bubble density of Cu film (Fig. 4a) and ΔH after irradiation (Fig. 4c) for individual Cu and V films are also shown. Reprinted with permission from E.G. Fu, A. Misra, H. Wang, L. Shao and X. Zhang, J. Nucl. Mater. 407 (2010). 178, © 2010 ELSEVIER BV.

diation hardening disappears. For a comparison at these figures the hardness values are given calculated from the additive considerations (Fig. 4c) and for the irradiated Cu and V films with 1 μm thickness (Fig. 4d). In summary, the results presented at Fig. 4 unambiguously manifest that in the multilayer films the swelling and radiation hardening are decreasing with the individual layers width, i.e. with the growth of the interface areas acting as the sinks for the radiation defects.

Some peculiarities of the hardness and the helium pores content in the Fe/W, Al/Nb and Cu/Nb multilayer films are investigated and discussed in details in works [31-33]. The nanostructure stability of the irradiated copper-based film alloys is studied in [34,35]. The temperature changes of the Mo and W nanosize inclusions into the as-deposited and irradiated $Cu_{90}Mo_{10}$ and $Cu_{90}W_{10}$ nanocomposite films are shown in Fig. 5 as well as the grain growth in the copper matrix [34]. The irradiation was carried out by Kr ions with energy 1.8 MeV having run range ~ 300 nm (the films thickness is ~ 200 nm). The irradiation dose was ~ 75 dpa (the fluence is $3x10^{12}$ ions/m^2). The data reflect the role of both an additional annealing and the irradiation temperature. As is illustrated in Fig. 5a, the Mo and W nanosize inclusions are nucleated and growing at temperatures ~ 400 °C and ~ 500 °C, correspondingly but their marked increase is detected at ~ 0.65 T_M and ~ 0.85 T_M (T_M – the copper melting point temperature). When the irradiation temperature is elevated from room temperature to 550 °C the inclusions size is increasing from ~3 to ~5 nm with the fast following growth for Mo, but only at T > ~800 °C for W. The authors of [34] have theoretically estimated the process of the Mo nanosize inclusions nucleation and growth under the thermal peaks action in the radiation displacement cascades and obtained a good agreement with the experimental data within the temperature range up to ~600 °C (solid curve at Fig. 5a).

The nanosize inclusions presence is favoring to a stability of the copper matrix nanostructure where the grain size at level below 40 nm remains practi-

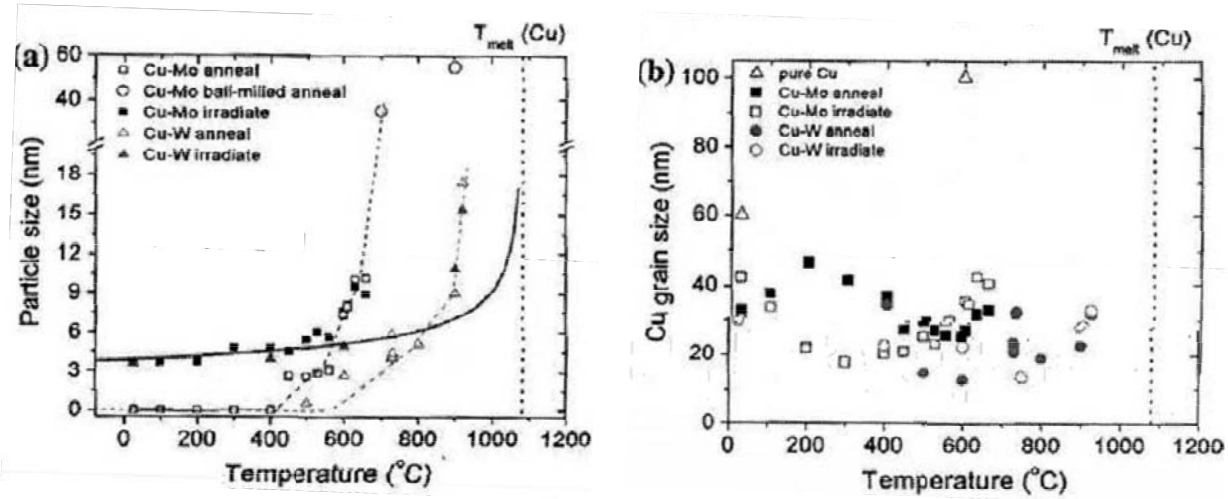

Fig. 5. The temperature influence on the nanoinclusions growth: (*a*) Mo and W (Δ – Cu-Mo (annealing); ○ – Cu-Mo (grinding + annealing); ■ – Cu-Mo (irradiation); □ – Cu-W (annealing); ▲ – Cu-W (irradiation) and the grain size growth of (b) copper matrix (Δ – Cu without additions; ■ – Cu-Mo (annealing); □ – Cu-Mo (irradiation); ● – Cu-W (annealing); ○ – Cu-W (irradiation) [34]. The solid curve at fig.5a shows the calculations of the Mo nanoinclusions growth under action of the thermal peaks; by the vertical dotted line the copper melting temperature is marked. Reprinted with permission from N.Q. Vo, S.W. Chee, D. Schwen, X. Zhang, P. Bellon and R.S. Averback, Scr. Mater. 63 (2010) 929, © 2010 PERGAMON.

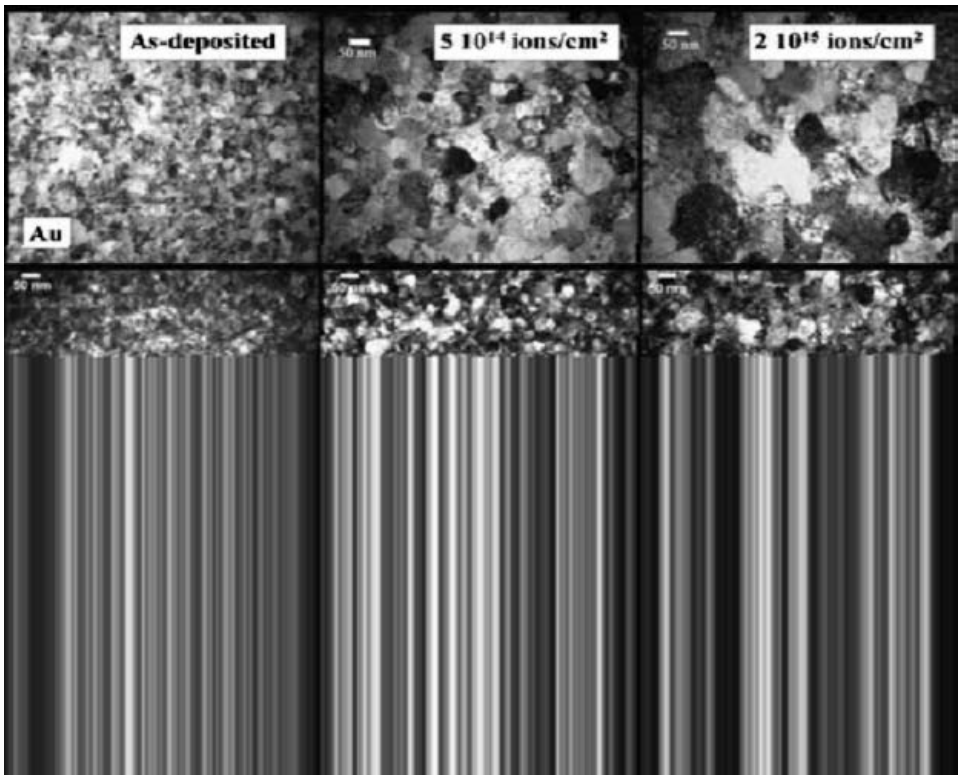

Fig. 6. Bright-field TEM-images of the Au, Pt and Cu films in the initial states and after an irradiation by the ions Ag (for aurum and platinum) and Kr (for copper) [36]. The scale mark is 50 nm. Reprinted with permission from D. Kaoumi, A.T. Motta and R.C. Birtcher, J. Appl. Phys. 104 (2008) 073525, © 2008 AMERICAN INSTITUTE OF PHYSICS.

cally unchangeable up to the annealing temperature 900 °C (Fig. 5b). At the same time, the annealing of the pure nanocrystalline copper at 600 °C leads to the grain sizes growth up to ~100 nm.

The peculiarities of the Kr ions irradiation influence on the decomposition of films from $Cu_{1-x}M_x$ type alloys (where $0.1 < x < 0.15$; M – Ag, Co, Fe, Mo, and Nb) and the changes of the mutual solubil-

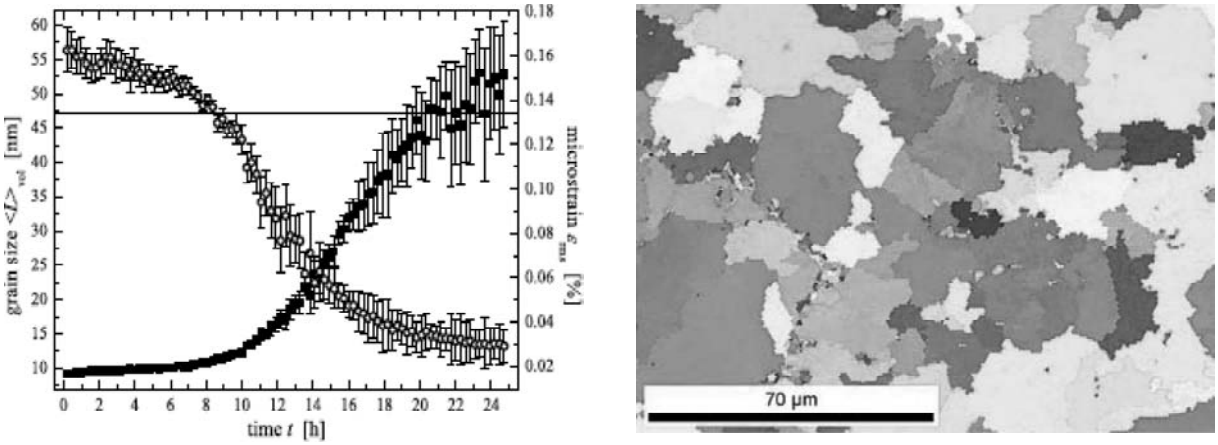

Fig. 7. The kinetics of the grain size changes (■) and the microscopic distortions (○) of the nanocrystaline palladium (*a*) and its microstructures after an ageing at the room temperatures during 60 days (*b*) [38]. The horizontal line corresponds to a limit grain size value fixes by the X-ray analysis. Reprinted with permission from M. Ames, J. Markman, R. Karos, A. Michels, A. Tschope and R. Birringer, Acta Mater. 56 (2008) 4255, © 2008 PERGAMON.

ity and sizes of nanoinclusions into the matrix nanostructure were analyzed in [35].

In work [36], the grains growth in the nanostructured metallic films (Au, Pt, Cu, Zr and Zr-Fe) was studied in detail under the irradiation by Ar (E = 0.5 MeV) and Kr (E = 0.5-1 MeV) ions. The nanostructure evolution presented in Fig. 6 for the irradiation fluence rise at room temperatures shows that the crystallite sizes are increasing in a wide temperature range including the low ones (20-773K). From these data the difference of the Au, Pt, and Cu films can be clearly connected with their melting point temperature differences. It is supposed to divide the temperature range tî three intervals: a pure thermal regime (where the temperature influence on the recrystallization is dominating), the thermo-induced (corresponding to a sum of the thermal and irradiation actions) and low-temperature (where the temperature influence is insignificant). The transition point from the low-temperature interval to the mixed one depends on the object, but in the mean over the homological scale is changing from 0.15 T_M to 0.20 T_M (T_M – melting point temperature). In the theory of the grains radiation-induced growth it is suggested that under an irradiation in the cascades and subcascades the thermal peaks are forming. On this base the ion irradiation-induced grain growth can be described by the relation of $L^n - L_o^n \sim K(Ft)$ type, where n~3, F – the beam intensity (ions/m^2·sec), t – time, K – a constant, depending on the grain mobility and driving force, L_o – the grain initial size.

It must be noted that in some studies under an irradiation not only the grain growth was observed but their size decrease too. Thus such effect was marked for the nickel samples with the initial nanostructure (with L_i = 115 nm) obtained by the intensive plastic deformations. After the irradiation by protons and nickel ions at room temperature (E_H = 590 MeV; dose 0.56 dpa; E_{Ni} = 590 keV) the grain mean size equals 38 nm [15, 37]. The same authors have observed the grain size growth from L_i = 178 nm to L = 493 nm under the irradiation of Cu-0.5Al_2O_3 samples. It can be added that the irradiation at 350 °C of the 316 stainless steel by Fe ions (E = 0.16 MeV, dose 5-10 dpa) was accompanied by the grain growth (L_o~40 nm and L~60 nm) [20]. At the same time the irradiation of Zr films by the high energy electrons (*Å*~1 MeV) had shown that even at 180 dpa the grain growth did not proceed [36]. It can be explained by the fact that the defect generation under the electron irradiation proceeds generally without cascade formation and their number is deficient (and mainly in the MAV forms) as distinct from the irradiations under the accelerator or reactor conditions.

The further study of the irradiation influence on the nanomaterial behavior (with account of the cascades overlapping and other factors) is important from the other point of view because the nanomaterial recrystallization can be accompanied with an abnormal grain growth and it can lead to the material degradation and the drastic decrease of its irradiation resistance and another physical and chemical properties. In Fig. 7 the grain growth kinetics and the microstresses fall at room temperatures are shown for a nanocrystalline Pd samples with the initial grain size ~7 nm and porosity ~4% [38]. As

Table 3. Irradiation effect on nanocrystals in amorphous SiO_2 matrix.

Subject	Size of nanocrystal (nm)	Irradiation conditions Ion	*Å* (MeV)	Dose (dpa); Fluence (ions/m^2)	Result
ZrO_2/SiO_2 [39]	~3	Xe	1	~0.8 dpa	Amorphization
ZrO_2 [46]	Single crystal	Xe	0.4	680 dpa	Crystal state
Cu/SiO_2 [40,41]	~2.5	Sn	5	0.16 dpa	Amorphization
	~8	Sn	5	10^{19}	Crystal state
Au/SiO_2 [39,42]	3	Xe	1	~0.8 dpa	Crystal state
	3-5	Sn	2.3	10^{19-20}	Crystal state
Ge/SiO_2 [43,44]	4-8	Si	5	10^{15-19}	Amorphization of nanocrystals is observed firstly
Co/SiO_2 [45]	3.7±1.0	Au	9	10^{17}	Amorphization

the data show, after about 8-hour conditioning there is observed a growth rate rise with the result that the nanostructure after 60 days turns into an usual microstructure with the grain sizes about 20-40 μm. It is obvious that any nanomaterial usage as the irradiation-resistant materials must take into account a possibility of such situation of the abnormal grain growth. In any case the methods of such effect prediction and guarding against must be developed.

Let us consider the data concerning the nanostructure amorphization under an irradiation action. Using the crystalline ZrO_2, Si, Cu, Co, and Ge nanoparticles, it was found that their irradiation into the inert matrixes (amorphous silicon oxide type) leads to an amorphization (e.g., see [39-45]). Some of the results presented in Table 3 were obtained using the nanocrystals implanted into the amorphous SiO_2 layers with thickness ~2 μm. The initial and irradiated nanocrystals state and compound was carried out using several methods (high resolution TEM, Rutherford backscattering, low-angle scattering, absorption X-ray spectroscopy, etc.) and the molecular dynamics modeling.

Especially characteristic results of Table 3 concern to the amorphization of zirconium oxide (which in single crystalline state is not amorphized even at the very high irradiation level doses [46]) and to the non-amorphized nanocrystals of gold and copper with dimensions about 8 nm. The experimental data [39,41,42] have shown that the dimensional factor (in the event of copper) and the irradiated nanocrystal nature (as in case of gold) have a pronounced influence on the process of the nanocrystalline state transformation into amorphous one under irradiation. The detailed study of the irradiated copper nanocrystals [41] has revealed also a role of Cu_2O formation in the amorphization process. The comprehensive description of the irradiated nanoparticles behavior (both in matrix and free) is given in review [47] where also some results are analyzed different from Table 3 results (for example, the results concerning cobalt nanocrystals) and is marked the necessity of the following investigations.

3. MODELLING AND MICROSCOPIC APPROACHES

The molecular dynamics methods (e.g., see [44, 45, 48-59], including the many scale methods [50, 53]) are widely used now for the nanomaterial behavior study under irradiation. Under the nanostructures irradiation by the high- energy ions and neutrons, the next situations were modeling: an amorphization of the irradiated nanocrystals in amorphous matrixes [44,45]; the displacement cascades into Ni nanograins (L = 5 and 12 nm) at bombarding particles energy of 5, 20, and 30 keV [48]; the radiation-stimulated grain growth of nanosize Ni particles (L = 5 and 10 nm) for cascade induced by a particle impact with energy 5 keV [49]; the interstitial atoms and tetrahedral stacking faults behavior into the damage cascades [50]; the evolution of the nanocrystalline film morphology under an irradiation [51,52]; the behavior under irradiation of the nanomaterials with the bcc- and fcc-structures [53]; the nucleation and growth of the vacancy clusters into a cubic modification of silicon carbide [55]; the grain boundaries behavior in the nanostructures acting as the defects sinks and sources [56], etc. In these works an important role of the grain inter-

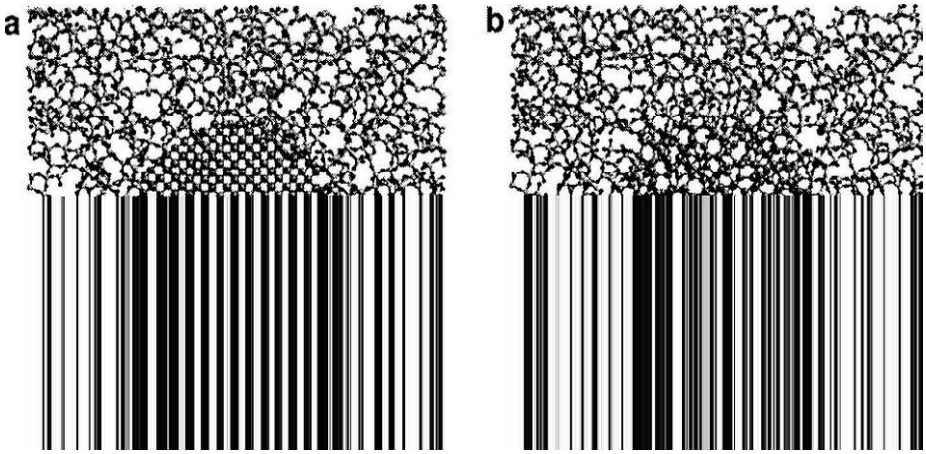

Fig. 8. The atomistic model of Ge-nanoparticle (the diameter of 4 nm) in amorphous SiC_2 matrix before (a) and after (b) high-doze irradiation [44]. Reprinted with permission from F. Djurabekova, M. Backman, O.H. Pakarinen, K. Nordlund, L.L. Araujo and M.C. Ridgway, Nucl. Instr. Meth. Phys. Res. B 267 (2009) 1235, © 2009 Elsevier Science.

faces and triple joints (as the radiation defect sinks) was demonstrated and the radiation-stimulated grain growth processes are studied in details as well as the corresponding changes of the surface roughness and stressed states. It is found that under the irradiation of the nanocrystalline materials with bcc- and fcc-structures the vacancy clusters are formed dominantly in the more loosen bcc-lattice. Fig. 8 shows the structures of nano-Ge/amorph SiO_2 system before and after ion irradiation [44,47]. the perfect crystal structure degradation of nano-Ge after irradiaton is obvious.

Let us consider in details the results of the cascade process modeling in vanadium [57] and copper [58,59]. The bcc-structured vanadium crystallites had the inclined Σ13<320>[001] and Σ17<410>[001] symmetric tilt grain boundaries with an atom numbers into the calculated cell from 65000 to 450000 in accordance with the PKA energy from <0.5 keV to >0.5 keV at temperature T = 10K [57]. The cascade evolution was studied for the three stages, namely the ballistic one (an energy propagation by the PKA atoms over the all volume of the model object with maximal number of the defects and the thermal peaks achieve), recombination one (the defect number decreases to a some stable value), and diffusion one (a following decrease of the defect number limited by their interaction and transport processes). The stimulation results have shown that the great interface surfaces sufficiently affect on the displacement cascade formation because the boundaries are accumulating the big part of the radiation defects and are preventing the cascade developing, being sometimes (depending on PKA values) even a non-permeable barrier for the cascades.

A modeling of the Frenkel pair IAV interaction with the grain boundaries for the fcc copper allows to suggest the next mechanism of this defect recombination: the boundaries are firstly saturated by the mobile interstitial atoms and after the saturation the inverse emission proceeds with a vacancy absorption in the boundary regions [58]. Representing the interface as a Σ11 <110> {131} symmetric tilt grain boundary and modeling a situation for 15 cascades (with the PKA kinetic energy 4 keV; the total atom number in system about 160.000, and the moving atoms number ~130.000), a temperature influence on the vacancy and interstitial atom removal along the grain interfaces was estimated. The calculation results have shown that in the 10-15K temperature range the process duration is very great ($t > 10^{10}$ sec) and no one of the mechanisms is relevant. In the range 70-100K (t < 1 sec) the interstitial atoms play the main role and at T = 300K all mechanisms for radiation defects are possible. These results allow to explain the experimental data shown in Fig. 9 concerning the electrical resistance of the irradiated Au foils with dimensions (width, length, height) of $0.5x10x5.3 \cdot 10^{-3}$ mm at temperatures 15K and 300K [60]. On the basis of resistance increments the results manifest that nanosize samples (L~23 nm), as compared with their coarse crystalline analogs, are more prone to an irradiation at low temperatures, when by an estimation of [58] all radiation defect removal mechanisms are not relevant. On the contrary, at the room temperatures (when all three mechanisms of the radiation defect

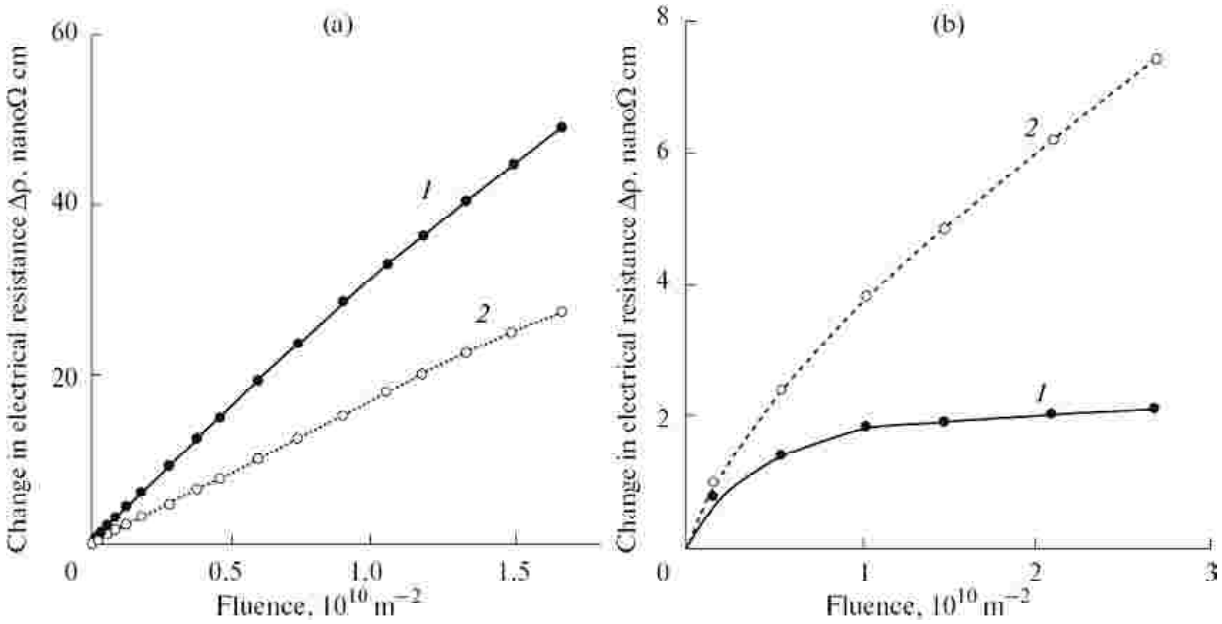

Fig. 9. The carbon atoms fluence (*Å* = 60 MeV) action on the electric resistance of the nanocrystalline (1) and coarse crystalline (2) Au samples at 15K (a) and 300K (b) [60]. Reprinted with permission from Y. Chimi, A. Iwase, N. Ishikawa, M. Kobiyama, T. Inami and S. Okuda, J. Nucl. Mater. 297 (2001) 355, © 2001 ELSEVIER BV.

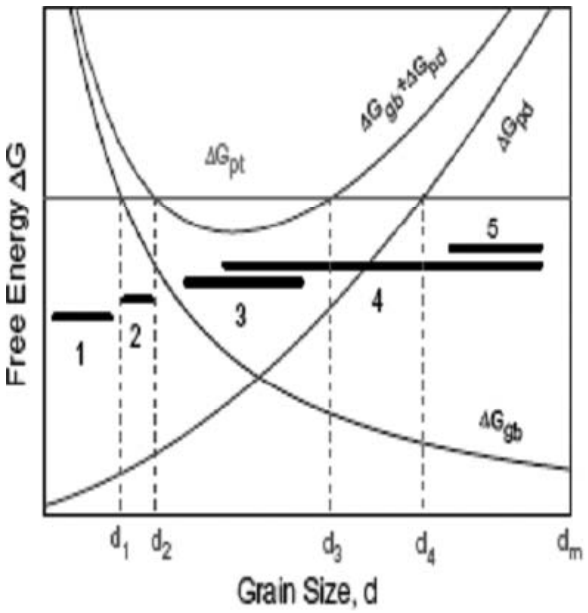

Fig. 10. The scheme of the grain size influence on the grain boundary interface free energy (ΔG_{gb}), the point effects free energy (ΔG_{pd}) and their summary value ($\Delta G_{gb}+\Delta G_{pd}$). The value ΔG_{am} is an amorphization energy barrier [62]. The (1-5) zone denotations are given in the text. Reprinted with permission from T.D. Shen, Nucl. Instr. Meth. Phys. Res. B 266 (2008) 921, © 2008 ELSEVIER BV.

removal are working) the nanostructure demonstrated the higher radiation stability.

The modeling of the competition processes of the radiation defect absorption by the grain boundaries and their volume recombination have shown that under the copper cascade-less irradiation by electrons at little times the accumulation of the Frenkel pairs IAV is progressing on the boundaries with the grain size decrease (in range from 40 nm to 15 nm), but subsequently the absorption by the bigger grains begins to prevail [59].

The microscopic approaches to the irradiation influence on the nanostructures were developed in works [61-63] where the Frenkel pairs IAV formation was studied for both highand low-energetic interactions. In former case the IAV were forming on the nanograin boundaries as well as into the grain itself, but in latter case – the vacancies arise only on the boundaries and the interstitial atoms arise into the grains [61]. The defects behavior evolution was analyzed for the next stages: 1) a radiation-induced defect generation; 2) the defects absorption by the boundaries between the grains; 3) the annihilation of IAV; 4) the stable clusters formation from the point defects. For the high-energetic interactions, stages 1) and 2) are assumed to be dominant. On the basis of the energy considerations a region of the advantaged amorphization was derived depending the nanograins size. From one side, the interfaces (grain boundaries) developed network is favorable for the excess free energy rise and is lowering the energy barrier of the amorphization, but from other side it is promoting the radiation defects removal, i.e. is preventing the amorphization.

The energetic approach was developed also in work [62], where a qualitative picture was presented for the free energy changes depending the nanograins size and a conclusion was drawn that for every material there is a special optimal grain size, providing the most effective amorphization resistance and the radiation defects removal. The results are shown schematically in Fig. 10, where the five zones are defined, taking into account the sums of the boundary grains and point defects free energies, as well as the barrier of amorphization (a transition from crystalline state to the amorphous one). These zones correspond to the next situations:

1. The transition to the amorphous state is possible without any irradiation ($L < L_1$), that is observed for example for the silicon nanoparticles with sizes below ~3 nm [64];
2. The transition to the amorphous state is initiated by a weak irradiation ($L_1 < L < L_2$);
3. In this size interval an irradiation doesn't lead to an amorphization ($L_2 < L < L_3$);
4. In this size interval an irradiation leads to an amorphization ($L_3 < L < L_4$);
5. In this size interval the defects free energy value is dominating and the boundaries play only a little role in the defects removal ($L_4 < L < L_{max}$). The defect annihilation by a volume recombination is prevailing at $L > L_{max}$.

The events in the 4 and 5 zones are qualitatively supported by above described results of ZrO_2 and Pd irradiation (Fig. 1) [8].

The peculiarities of the radiation defect formation in nanocrystals being inserted into an inert solid-body matrix have been analyzed in work [63]. It was shown that the crystalline nanocluster amorphization into an inert matrix may be either accelerated (a radiation damage) or slowed-down (a radiation resistance). These variants realization depends on the situation at the interface nanocluster–matrix, which can be (as compared with the coarse crystalline objects) either compressed (the accelerated amorphization) or extended (the retarded defect formation). These results qualitatively correspond to the data of Table 3 but it is hard to derive the more correct information for the many factors influence and various assumptions.

4. CONCLUSIONS

The presented data clearly demonstrate that the interfaces play an important role in the consolidated nanomaterial characteristics and a rise of their radiation stability. This fact gives a serous orientation in the practical design of the new materials especially for the nuclear and thermonuclear power engineering but, in spite of the currently rising interest to the nanomaterial radiation stability, many aspects of this problem invite further investigations. The first question is connected with the radiation defects nature and their evolution in dependence of the irradiation dose, annealing temperature, stressed state and environment conditions. In this connection it should be noted that the radiation processes of the nanostructures stabilization, amorphization and recrystallization have a very important role that must be carefully investigated for the materials behavior prediction and control.

It is obvious that the technologies of the future radiation resistant materials will have a crucial importance. The further improvements of the technology regimes must provide a production of the stable nanostructured materials with high physical-mechanical and physical-chemical properties along with their economical efficiency. It must be also noted that above analyzed questions are far from exhausting all the problems connected with the nanomaterials radiation resistance. There are many related problems: a hydrogen behavior into the irradiated nanostructures and their erosion (e.g., see [65,66]), the radiation influence on the nanocrystallization in metallic glasses [67,68] and a nanodomain formation under the metastable alloys irradiation [69,70]. More over the radiation stability problems exist not only for the main constructional materials used in the nuclear and thermonuclear power engineering but also for many auxiliary objects (scintillation counters, sensors, cosmic units, etc.). The frames of this survey don't allow consider all the problems but a necessity of the general approach to the radiation defects behavior in irradiated nanomaterials designed for the various purposes or in the relative objects. Some questions on the radiation stability of nanomaterials are also discussed in author's review [71].

ACKNOWLEDGEMENTS

The author is grateful to Profs. A. Didyk, S. Golubov, I. Ovid'ko, V. Sagaradze, and X. Zang for discussions on radiation damage and paper sending. This work was supported by the Program for Fundamental Researches of the RAS Presidium (P21) and by the Russian Foundation for Basic Research (Projects No 09-08-11005 and No 08-03-00105).

REFERENCES

[1] R.A. Andrievski // *Russ. Chem. Rev.* **71** (2002) 967.

[2] R.A. Andrievski // *J. Mater. Sci.* **38** (2003) 1367.
[3] I.A. Ovid'ko // *Mater. Phys. Mech.* **8** (2009) 174, In Russian.
[4] R.A. Andrievski // *Phys. Met. Metalogr.* **110** (2010) 229.
[5] Yu.V. Trushin, *Radiation Processes in Multicomponent Materials. Theory and Computer Modelling* (Ioffe Physical Technical Institute, Sankt Petersburg, 2002), in Russian.
[6] S.I. Golubov, A.V. Barashev and R.E. Stoller, In: *Encyclopedia of Comprehensive Nuclear Materials*, ed. by R. Konigs (Elsevier, Amsterdam, 2011), chapter 29 "Radiation Damage Theory".
[7] S. Wurster and R. Pippan // *Scr. Mater.***60** (2009) 1083.
[8] M. Rose, G. Gorzawski, G. Miehe, A.G. Balogh and H. Hahn // *Nanostr. Mater.* **6** (1995) 731.
[9] M. Rose, A.G. Balogh and H. Hahn // *Nucl. Instr. Meth. Phys. Res. B* **127/128** (1997) 119.
[10] T.D. Shen, Sh.Feng, M. Tang, J.A. Valdez, Y. Wang and K.E. Sicafus // *Appl. Phys. Lett.***90** (2007) 263115.
[11] A.R. Kilmametov, D.V. Gunderov, R.Z. Valiev, A.G. Balogh and H. Hahn // *Scr. Mater.* **59** (2008) 1027.
[12] Y. Leconte, I. Monnet, M. Levalois, M. Morales, X. Portier, L. Thome, N. Herlin-Boime and C. Reynaud, In : *Mater. Res. Soc. Symp.Proc. V. 981* (Warrendale, MRS, 2007), p. JJ07.
[13] H. Kurushita, S. Kobayashi, K. Nakai, T. Ogawa, A. Hasegawa, K. Abe, H. Arakawa, S. Matsuo, T. Takida, K. Takebe, M. Kawai and N. Yoshida // *J. Nucl. Mater*.**377** (2008) 34.
[14] D.A. McClintock, D.T. Hoelzer, M.A. Sokolov and R.K. Nanstad // *J. Nucl. Mater*. **386-388** (2009) 307.
[15] N. Nita, R. Schaeublin, M. Victoria and R.Z. Valiev // *Phil. Mag*.**85** (2005) 723.
[16] H. Matsuoka, T. Yamasakl. Y.J. Zheng, T. Mitamura, M. Teresawa and T. Fukami // *Mater. Sci. Eng. A* **449** (2007) 790.
[17] D.A. McClintock, M.A. Sokolov, D.T. Hoelzer and R.K. Nanstad // *J. Nucl. Mater.* **392** (2009) 353.
[18] P. Miao, G.R. Odette, T. Yamamoto, M. Alinger and D. Klingensmith // *J. Nucl. Mater.* **377** (2008) 59.
[19] G.R. Odette, M.J. Alinger and B.D. Wirth // *Ann. Rev. Mater. Res.* **38** (2008) 471.
[20] B. Radiguet, A. Etienne, P. Pareige, X. Sauvage and R. Valiev // *J. Mater. Sci.* **43** (2008) 7343.
[21] S.V. Rogozhkin, A.A. Aleev, A.G. Zaluzhnyi, A.A. Nikitin, N.A. Iskandarov, P. Vladimirov, R. Lindau and A. Moslang // *J. Nucl. Mater.* **409** (2011) 94.
[22] G.V. Lysova and G.A. Birzevoy // *Bull. Russ. Acad. Sci.: Physics* **74** (2010) 135.
[23] http://www.bochvar.ru
[24] I.I. Ivanova and A.N. Demidik // *Powder Metall. Metal Ceram.* **7/8** (2010) 96 (English transl.).
[25] V.L. Arbuzov, B.N. Goschitskiy, V.V. Sagaradze, S.E. Danilov and A.E. Kar'kin // *Phys. Met. Metallogr.* **110** (2010) 384.
[26] V.V. Sagaradze, V.A. Pavlov, V.M. Alyab'ev, S.S. Lapin, V.A. Ermishkin and O.V. Antonova // *Phys. Met. Metallogr.* **64** (1987) 966.
[27] V.V. Sagaradze and S.S. Lapin // *Phys. Met. Metallogr.* **83** (1997) 129.
[28] H. Wang, R. Araujo, J.G. Swadener, Y.Q. Wang, X. Zhang, E.G. Fu and T. Cagin // *Nucl. Instr. Meth. Phys. Res. B*.**261** (2007) 1162.
[29] M. Popović, M. Novacović and N. Bibić // *Mater. Character.* **60** (2009) 1463.
[30] E.G. Fu, A. Misra, H. Wang, L. Shao and X. Zhang // *J. Nucl. Mater.* **407** (2010). 178.
[31] N. Li, E.G. Fu, H. Wang, J.J. Carter, L. Shao, S.A. Maloy, A. Misra and X. Zhang // *J. Nucl. Mater.* **389** (2009) 233.
[32] N. Li, M.S. Martin, O. Anderoglu, A. Misra, L. Shao, H. Wang and X. Zhang // *J. Appl. Phys.* **105** (2009) 123522.
[33] A. Misra, M.J. Demkowicz, X. Zhang and R.G. Hoagland // *JOM.* **52** (2007) 62.
[34] N.Q. Vo, S.W. Chee, D. Schwen, X. Zhang, P. Bellon and R.S. Averback // *Scr. Mater.* **63** (2010) 929.
[35] S.W. Chee, B. Stumphy, N.Q. Vo, R.S. Averback and P. Bellon // *Acta Mater.* **58** (2010) 4088.
[36] D. Kaoumi, A.T. Motta and R.C. Birtcher // *J. Appl. Phys.* **104** (2008) 073525.
[37] N. Nita, R. Schaeublin and M. Victoria // *J. Nucl. Mater.* **329-333** (2004) 953.
[38] M. Ames, J. Markman, R. Karos, A. Michels, A. Tschöpe and R. Birringer // *Acta Mater.* **56** (2008) 4255.

[39] A. Meldrum, L.A. Boatner and R.C. Ewing // *Phys. Rev. Lett.* **88** (2002) 025503.
[40] B. Johannessen, P. Kluth, D.J. Liewellyn, G.J. Foran, D.J. Cookson and M.C. Ridgway // *Appl. Phys. Lett.* **90** (2007) 073119.
[41] B. Johannessen, P. Kluth, D.J. Liewellyn, G.J. Foran, D.J. Cookson and M.C. Ridgway // *Phys. Rev. B* **76** (2007) 184203.
[42] P. Kluth, B. Johannessen, G.J. Foran, D.J. Cookson, S.M. Kluth and M.C. Ridgway // *Phys. Rev. B* **74** (2006) 014202.
[43] M.C. Ridgway, G.M. Azevedo, R.G. Elliman, C.J. Glover, D.J. Liewellyn, R. Miller, W. Wesch, G.J. Foran, J. Hansen and A. Nylandsted-Larsen // *Phys. Rev. B* **71** (2005) 094107.
[44] F. Djurabekova, M. Backman, O.H. Pakarinen, K. Nordlund, L.L. Araujo and M.C. Ridgway // *Nucl. Instr. Meth. Phys. Res. B* **267** (2009) 1235.
[45] D.J. Sprouster, R. Giulian, L.L. Araujo, P. Kluth, B. Johannessen, N. Kirby, K. Nordlund and M.C. Ridgway // *Phys. Rev. B* **81** (2010) 155414.
[46] K.E. Sickafus, H. Matzke, Th. Hartman, K. Yasuda, P. Valdez, I. Chodak, M. Nastasi and R.A. Verral // *J. Nucl. Mater.* **274** (1999) 66.
[47] A.V. Krasheninnikov and K. Nordlund // *Appl. Phys. Rev.* **107** (2010) 071301.
[48] M. Samaras, P.M. Derlet, H. Van Swygenhoven and M. Victoria // *Phys. Rev. Lett.* **88** (2002) 125505.
[49] W. Voegeli, K. Albe and H. Hahn // *Nucl. Instr. Meth. Phys. Res. B* **202** (2003) 230.
[50] M. Samaras, P.M. Derlet, H. Van Swygenhoven and M. Victoria // *J. Nucl. Mater.* **323** (2003) 213.
[51] S.G. Mayr and R.S. Averback // *Phys. Rev. B* **68** (2003) 075419.
[52] S.G. Mayr, Y. Ashkenazy and R.S. Averback // *Nucl. Instr. Meth. Phys. Res. B* **212** (2003) 246.
[53] M. Samaras, P.M. Derlet, H. Van Swygenhoven and M. Victoria // *J. Nucl. Mater.* **351** (2006) 47.
[54] P.C. Millett, D. Wolf, T. Desai and V. Yamakov // *Appl. Phys. Lett.* **93** (2008) 161902.
[55] K. Morishita, Y. Watanabe, A. Kohyama, H.L. Heinisch and F. Gao // *J. Nucl. Mater.* **386-388** (2009) 30.
[56] P.C. Millet, D.S. Aidhy, T. Desai, S.R. Phillpot and D. Wolf // *Int. J. Mater. Res.* **100** (2009) 550.
[57] S.G. Psakh'e, K.P. Zol'nikov, D.S. Kryzhevich, A.V. Zheliazniakov and V.M. Chernov // *Crystallography Reports* **54** (2009) 1053.
[58] X.-M. Bai, A. F. Voter, R.G. Hoagland, M. Nastasi and B.P. Uberuaga // *Science* **327** (2010) 1631.
[59] Y. Yang, H. Huang and S.J. Zinkle // *J. Nucl. Mater.* **405** (2010) 261.
[60] Y. Chimi, A. Iwase, N. Ishikawa, M. Kobiyama, T. Inami and S. Okuda // *J. Nucl. Mater.* **297** (2001) 355.
[61] I.A. Ovid'ko and A.G. Sheinerman // *Appl. Phys. A* **81** (2005) 1083.
[62] T.D. Shen // *Nucl. Instr. Meth. Phys. Res. B* **266** (2008) 921.
[63] B.L. Oksengendler, N.N. Turaeva, S.E. Maximov and F.G Djurabekova // *J. Exp. Theor. Phys.* **138** (2010) 469.
[64] T.D. Shen, C.C. Koch, T.L. McCormick, R.J. Nemanich, J.Y. Huang and J.G. Huang // *J. Mater. Res.* **10** (1995) 139.
[65] V.L. Arbuzov, B.N. Goshcitskiy, S.E. Danilov, Ju.N. Zuev, A.E. Kar'kin and V.V. Sagaradze // *Phys. Met. Metalogr.* **109** (2010) 326 (English transl.).
[66] V.I. Krauz, Ju.V. Martynenko, N.Ju. Sveshnikov, V.P. Smirnov, V.G. Stankevich and L.N. Khimchenko // *Physics – Uspekhi* **53** (2010) 1015.
[67] J. Carter, E.C. Fu, M. Martin, G. Xie, X. Zhang, Y.Q. Wang, D. Wijesundera, X.M. Wang, W.-K. Chu, S.M. McDeavitt and L. Shao // *Nucl Instr. Meth. Phys. Res. B* **267** (2009) 2827.
[68] R.A. Andrievski // *Bull. Russ. Acad. Sci. Physics* **76** (2012) No 1, accepted for publication.
[69] V.S. Khmelevskaya, A.V. Nakin and V.G. Malynkin // *Izvestia VUZOV. Physica* **No 6** (2001) 33, In Russian.
[70] V.P. Kolotushkin, C.N. Votinov and C.A. Nikulin // *Metals*. **No 3** (2009) 74, In Russian.
[71] R.A. Andrievski // *Nanotechnologies in Russia* **6** (2011) 257.